

# Theoretical prediction of antiferromagnetism in layered perovskite Sr<sub>2</sub>TcO<sub>4</sub>

Alen Horvat,<sup>1</sup> Leonid Pourovskii,<sup>2</sup> Markus Aichhorn,<sup>3</sup> and Jernej Mravlje<sup>1</sup>

<sup>1</sup>*Jožef Stefan Institute, Jamova 39, Ljubljana, Slovenia*

<sup>2</sup>*Centre de Physique Théorique, École Polytechnique, CNRS, 91128 Palaiseau Cedex, France*

<sup>3</sup>*Institute of Theoretical and Computational Physics, TU Graz, Petersgasse 16, Graz, Austria*

We theoretically investigate magnetic properties of Sr<sub>2</sub>TcO<sub>4</sub>, a 4d transition-metal layered perovskite of the K<sub>2</sub>NiF<sub>4</sub>-type with half-filled t<sub>2g</sub> states. The effect of local Coulomb repulsion between the t<sub>2g</sub> orbitals is included within the density-functional theory (DFT)+U and DFT+dynamical mean-field theory (DMFT) methods. The DFT+DMFT predicts paramagnetic Sr<sub>2</sub>TcO<sub>4</sub> to be close to the Mott insulator-to-metal transition, similarly to the cubic compound SrTcO<sub>3</sub>. The inter-site exchange interactions computed within the DFT+DMFT framework point to a strong antiferromagnetic coupling between the neighboring Tc sites within the layer. We then evaluate the Néel temperature  $T_N$  within a classical Monte Carlo approach including dipolar interactions, which stabilize the magnetic order in the frustrated K<sub>2</sub>NiF<sub>4</sub> lattice structure. Our approach is applied to a set of layered and cubic perovskites. The obtained  $T_N$  are in fair agreement with experiment. Within the same approach we predict  $T_N$  of Sr<sub>2</sub>TcO<sub>4</sub> to be in the 500-600 K range.

## I. INTRODUCTION

Recently, antiferromagnetism persisting to high temperatures has been found in Tc<sup>4+</sup> perovskites SrTcO<sub>3</sub> and CaTcO<sub>3</sub>.<sup>1,2</sup> In 4d oxides the magnetism is found less often than in more localized 3d oxides, hence strong magnetic properties were not anticipated. As technetium is radioactive, Tc perovskites have not been intensely experimentally investigated. Encountering a new class of compounds in a familiar perovskite lattice with little experimental information provides a unique opportunity to test theoretical tools. In this paper we theoretically investigate magnetic properties of layered perovskite Sr<sub>2</sub>TcO<sub>4</sub>.

What makes Tc perovskites special among 4d compounds is that they have a half-filled t<sub>2g</sub> shell.<sup>3</sup> Several theoretical works<sup>1,4,5</sup> discussed the role of more extended 4d orbitals, which give rise to a large hybridization and small values of Hubbard interaction compared to the 3d elements, and hence strong exchange interactions. Nevertheless, in addition to Refs. 1, 4, and 5 most of the recent work<sup>6-8</sup> recognized that electronic correlations remain sizable in Tc compounds, too; if the interactions were too small, the localized magnetic moments would not establish. The key ingredient, that helps localization is the Hund's rule coupling,<sup>9</sup> that for the half-filled shell increases the cost of charge excitations.<sup>3</sup> As a joint result of the Hund's rule coupling and the more extended 4d orbitals, the Tc compounds are situated right at the itinerant-to-localized transition<sup>3</sup> where the Néel temperatures are maximal.<sup>5</sup> Other 4d oxides do not have half-filled shells<sup>9</sup> and, consequently, rarely exhibit ordered antiferromagnetism.

A layered Tc<sup>4+</sup> perovskite, Sr<sub>2</sub>TcO<sub>4</sub>, has been synthesized,<sup>10</sup> too. It crystallizes in the layered body-centered tetragonal K<sub>2</sub>NiF<sub>4</sub>-type lattice, with the lattice constants  $a = 3.902 \text{ \AA}$ ,  $c = 12.72 \text{ \AA}$ , and space group I4/mmm.<sup>10,11</sup> To our knowledge, only its basic crystal structure has been reported, but more detailed measurements, in particular, the determination of the magnetic

structure, have not been performed to date.

From the similarity with the cubic SrTcO<sub>3</sub> one may expect sizable magnetic interactions also in the layered Sr<sub>2</sub>TcO<sub>4</sub>,<sup>6</sup> but the question of the long-range ordering in layered systems is more subtle,<sup>12</sup> in particular for the lattices of the K<sub>2</sub>NiF<sub>4</sub>-type. Usually, in quasi-2D the transition temperatures are not suppressed so much with respect to the 3D lattices. The magnetic susceptibility in 2D increases exponentially on cooling down.<sup>13</sup> The usual argument then implements the inter-plane exchange interaction  $J_{\perp}$  at the mean-field level,<sup>14,15</sup> which leads to only logarithmic suppression of the ordering temperature  $T_c \sim T_c^{3D} / \log(bJ/J_{\perp})$  with diminishing  $J_{\perp}$  ( $b$  is model dependent number).<sup>13,16</sup> In the present case of the body-centered K<sub>2</sub>NiF<sub>4</sub> structure, however, the frustration suppresses the effective coupling between layers completely, provided the in-plane order is checkerboard antiferromagnetic. When this is the case (as it turns out to be in Sr<sub>2</sub>TcO<sub>4</sub>), each spin is equally coupled to the same number of oppositely oriented spins in the layer above (and likewise below), hence the net inter-plane coupling cancels out. Nevertheless, the antiferromagnetic order is experimentally found also in lattices of this kind, for instance in K<sub>2</sub>NiF<sub>4</sub><sup>17</sup> and Rb<sub>2</sub>MnF<sub>4</sub>.<sup>18</sup> The reason can be traced to the magnetic anisotropies that originate in the dipole-dipole interactions.<sup>17-20</sup> If a pair of magnetic moments is forced to point in opposite directions by a strong antiferromagnetic exchange, the dipole-dipole energy is reduced when the moments are oriented perpendicular to the line connecting them. In a planar configuration with antiferromagnetic arrangement of nearest neighbors, the moments will prefer to point in a direction perpendicular to the plane. Such effective anisotropy in the presence of a long in-plane correlation length is sufficient to stabilize the order already in a single layer. Once the order is established in 2D, the long-range order in 3D follows due to any non-vanishing next-nearest layer coupling.

In the present work we study theoretically the electronic structure and magnetic properties of Sr<sub>2</sub>TcO<sub>4</sub>. We calculated the exchange interactions using a linear-

response approach based on DFT+DMFT and found a large antiferromagnetic coupling between the nearest neighboring Tc moments. In order to determine the Néel temperature, we employed a classical spin Monte Carlo technique with dipole-dipole interactions included.<sup>21,22</sup> We tested our approach on a set of layered and cubic perovskites, for which the experimental values of exchange parameters are known. This allows us to estimate systematic errors of our theoretical exchange interactions. With a correction for this systematic error included, we predict the transition temperature of Sr<sub>2</sub>TcO<sub>4</sub> to be about 500 K.

The paper is structured as follows. In Sec. II we describe our theoretical approach. In Sec. III we present our DFT+U and DFT+DMFT results from which we infer the magnetic ordering. In Sec. III C we report the results of the calculated exchange interactions and transition temperatures for a set of perovskites including the predicted value for Sr<sub>2</sub>TcO<sub>4</sub>. The relevance of effects that were not included in our results is discussed in Sec. IV. Appendix A gives further details of the calculation of exchange interactions.

## II. METHODS

### A. DFT+U

We have employed a rotationally invariant DFT+U implementation of the Wien2k package,<sup>23</sup> and used  $U_{\text{eff}} = U - J = 2.04$  eV as the value for the Coulomb repulsion.<sup>24</sup> The double-counting correction term<sup>25</sup> was taken in the fully-localized limit, and we used the generalized-gradient approximation (GGA)<sup>26</sup> as approximation to the exchange correlation potential. The Brillouin zone (BZ) integration was carried out with 1000  $\mathbf{k}$ -points in the full BZ, which corresponded to 56 (150)  $\mathbf{k}$ -points in the tetragonal (orthorhombic) irreducible BZ. The muffin-tin (MT) radii were fixed at 1.81, 2.1 and 1.6 a.u. for Tc, Sr and O, respectively, in all total energy and structural relaxation calculations.

### B. DFT+DMFT

The influence of electronic correlations was also investigated within the DFT+DMFT approach. We use the efficient implementation of this method as provided by the TRIQS package.<sup>27–29</sup> Based on DFT calculations within the local-density approximation (LDA) using Wien2k, we construct Wannier functions for the  $t_{2g}$  orbitals, which serve as a basis for the DMFT calculations. The solution of the DMFT quantum impurity problem was done by a continuous-time quantum Monte Carlo (CTQMC) method in hybridization expansion<sup>30–32</sup> including full rotational invariant interactions.<sup>33</sup> We use the same interaction values  $U = 2.3$  eV and  $J_H = 0.3$  eV as previously for SrTcO<sub>3</sub>.<sup>5</sup> We performed paramagnetic and magnetic

calculations. For the magnetic calculation, we used unit cell that could accommodate the G-type ordering pattern, which is a checkerboard AFM in the plane and FM stacking in  $c$  direction in the unit cell containing two oppositely oriented Tc<sup>4+</sup> spins. In the paramagnetic calculation, standard tetragonal unit-cell was used and the self-energies were spin-symmetrized after each iteration of the DMFT loop.

### C. Calculation of exchange interactions

In order to calculate the magnetic transition temperature we define an effective Hamiltonian associated with magnetic degrees of freedom. In Mott insulators this Hamiltonian is known to be well approximated by the quantum Heisenberg form

$$\mathcal{H} = -\frac{1}{2} \sum_{i \neq j} J_{ij} \hat{\mathbf{S}}_i \cdot \hat{\mathbf{S}}_j, \quad (1)$$

where  $\hat{\mathbf{S}}$  are spin operators and  $J_{ij}$  are inter-site exchange interactions. We denote  $J_{i,j} = J$  for nearest neighbor interactions.

The inter-site exchange interactions were extracted from the results of DFT+DMFT calculations within the Hubbard-I<sup>34</sup> approximation (DFT+HubI) using an approach similar to the DFT-based linear response techniques introduced in Refs. 35–37 (and generalized to DFT+DMFT in Refs. 38 and 39). Similarly to those techniques, our approach is based on evaluating a linear response to simultaneous magnetic fluctuations on two neighboring sites. The standard “Lichtenstein interactions”<sup>35,36</sup> and their DFT+DMFT generalizations are derived by considering simultaneous tilting of two moments in a magnetically-ordered ground state. In contrast, we compute inter-site exchange interactions from a local-moment paramagnetic state (described within Hubbard-I), which is advantageous when the ground-state magnetic order is not known. More details follow in Appendix A.

### D. Mapping to the classical spin Heisenberg model

We approximate the quantum Heisenberg model Eq. (1) with the classical one:

$$\mathcal{H}_c = -\frac{1}{2} \sum_{i \neq j} J_{ij} \alpha \mathbf{S}_i \cdot \mathbf{S}_j. \quad (2)$$

$\mathbf{S}_i$  are three-dimensional vectors of length unity and constant  $\alpha$  keeps track of the length of the quantum spin. It has to be adjusted in a way that the classical model gives the best approximation to the quantum model.

As  $\hat{S}^2 = S(S+1)$  (with  $S = 3/2$  in the ground state of the Tc ion) suggests  $\alpha_1 = S(S+1)$  should be used. Indeed, largest deviations from the classical results are

expected for  $S = 1/2$  and even there the choice  $\alpha_1$  gives for the simple cubic lattice in 3D results that differ from the quantum ones only by about 15%.<sup>16,40,41</sup>

One can rationalize also a different choice of  $\alpha$ . Consider a pair of magnetic moments and compare the energy of parallel and anti-parallel configurations. For quantum spins, the energy difference is  $\Delta E = JS(2S + 1)$ , which follows from comparing the expectation value

$$J\langle\hat{\mathbf{S}}_i \cdot \hat{\mathbf{S}}_j\rangle = J[S'(S'+1) - S_i(S_i+1) - S_j(S_j+1)]/2, \quad (3)$$

in the singlet configuration (where the spin of the pair is  $S' = 0$ ) with the triplet configuration ( $S' = 2S$ ) of the pair. For the classical model, the corresponding energy difference is simply  $2J_c$  (denoting the classical exchange as  $J_c$ ). Comparing the two results, leads to a choice  $\alpha_2 = S(S + 1/2)$ . A third choice  $\alpha_3 = S^2$  is also used in the literature.<sup>42,43</sup>

The experiment suggests that the choice  $\alpha_1$  is the best one. Namely, in several cases, where the exchange constants have been measured experimentally, the calculated values of transition temperatures agree best with the observed ones if  $\alpha_1$  is used, see Sec. III and Ref. 18 and 43. (Note, that in Ref. 43, experimental exchange constants have been rescaled according to  $\alpha_3$ .)

However, quite universally the numerical approaches overestimate the exchange interactions.<sup>4,39</sup> We find this holds for our results, too. In such cases, a smaller choice of  $\alpha$  than  $\alpha_1$  improves the agreement with the experiment. Hence, in the following paper we give our results for all of the three mappings, together with the known experimental results for easy comparison.

To correctly describe magnetic properties of the layered perovskites one needs to take into account additionally long-range dipolar interactions and/or single-ion anisotropy as will be discussed in more detail later.

### E. Monte Carlo simulations

We describe the cubic perovskites with the isotropic Heisenberg model Eq. (2). We implemented two algorithms: the modified Wolff cluster algorithm,<sup>22</sup> which is applicable whenever spin frustration is weak, and the Metropolis-Hasting algorithm with over-relaxation.<sup>21</sup> For the data described in the paper, the two algorithms gave consistent results.

For layered perovskites of the  $\text{K}_2\text{NiF}_4$ -type, the dipole-dipole magnetic interactions are crucial to explain finite Néel temperatures. Therefore, we add to the short-range Heisenberg-type classical Hamiltonian Eq. (2) a contribution from long-range dipolar interactions. The resulting total Hamiltonian reads

$$\mathcal{H}' = \mathcal{H}_c + \frac{\tilde{\mu}S^2}{2} \sum_{i \neq j} r_{ij}^{-3} [\mathbf{S}_i \cdot \mathbf{S}_j - 3(\mathbf{S}_i \cdot \hat{\mathbf{r}}_{ij})(\mathbf{S}_j \cdot \hat{\mathbf{r}}_{ij})]. \quad (4)$$

We denote  $\tilde{\mu} = (g\mu_B)^2\mu_0/(4\pi) = 0.214 \text{ meV}\text{\AA}^3$ ,  $g \approx 2$  is the Landé factor,  $\mu_B$  is the Bohr magneton and  $\mu_0$  is

the permeability constant. The dipolar term scales as  $S^2$ , since the energy of a spin with a magnetic moment  $g\mu_B S$  in a dipolar field generated by a spin with the same magnetic moment is proportional to  $S^2$ .<sup>18</sup>

Magnetic ions in the  $\text{K}_2\text{NiF}_4$  structure form a body-centered tetragonal unit cell. Energy contributions of spins in the center of the unit cell to a spin in the corner of the unit cell cancel due to frustration. Hence we disregard the central ions and the remaining ions form a simple cubic tetragonal unit cell. Two layers of spins with long-range dipole-dipole interactions Eq. (4) and with open boundary conditions in  $z$  direction are simulated as in Ref. 18. Dipole-dipole interactions were included up to fifth nearest neighbor. We checked that the results do not change if the range of the dipole-dipole interaction is increased further.

## III. RESULTS

### A. DFT+U

We have considered three kinds of magnetic ordering: ferromagnetic (FM) ordering as well as A-type and G-type antiferromagnetic (AFM) ordering. The A-type AFM structure has the tetragonal P4/mmm space group with the Tc moments aligned ferromagnetically within (001) planes and antiferromagnetically between the neighboring planes. The G-type structure has a doubled unit cell of orthorhombic Cmmm space group, with the moments of Tc in the center of the  $ab$  face being anti-parallel to those of Tc in the vertices.

The calculated total energy of the AFM G-type phase at the experimental lattice parameters<sup>10</sup> is 0.41 eV below those of the FM and AFM A-type ones. The total energy of the A-type phase is just 5 meV below the FM's one. Because the moments of nearest neighbor Tc ions are aligned ferromagnetically in the FM and AFM A-type structures, but antiferromagnetically in the G-type AFM one, we conclude that a very strong nearest-neighbor AFM coupling is by far the most significant magnetic interaction in this system. Longer-range interactions are weaker. For example, the second nearest-neighbor interaction (the one between Tc moment in the corner and in the center of the tetragonal cell) gives opposite sign contributions to the energies of the FM and A-type phases that are almost degenerate in the present case.

The G-type AFM is clearly the lowest-energy structure among all considered, and its large stabilization energy with respect to the other two phases can hardly be offset by lattice relaxations. Therefore, we performed lattice structure optimization for the AFM G-type phase only. We have found that orthorhombic distortions due to the G-type ordering are negligible, and performed the full optimization of the  $a(=b)$ ,  $c$  and internal coordinates. As one may see in Fig. 1 the theoretical equilibrium volume is 3% larger than the experimental one due to the usual tendency of GGA towards a volume overestimation. The

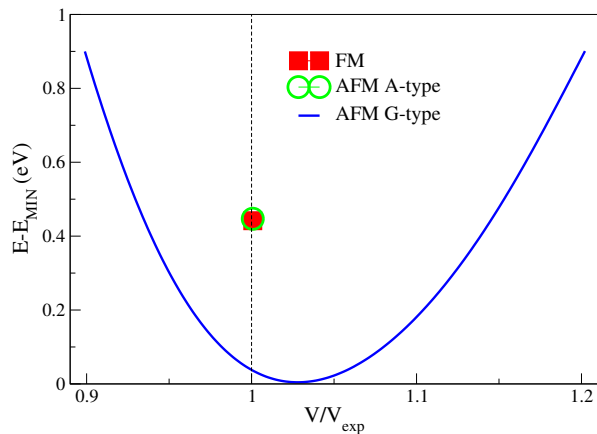


Figure 1. Solid line: the total energy vs. volume for the fully-relaxed AFM G-type structure of  $\text{Sr}_2\text{TcO}_4$ . The square and the circle indicate the total energies of the FM and AFM A-type structures, respectively.

DFT+U equilibrium lattice parameters  $a(=b)$  and  $c$  of the Cmmm structure are  $5.61 \text{ \AA}$  and  $12.68 \text{ \AA}$ , respectively. There are two distinctive  $z_{\text{Sr}}$  and three distinctive  $z_{\text{O}}$  in the Cmmm structure due to symmetry lifting. However, the difference between the optimized values of the corresponding  $z$  parameters is very small (below 0.1%) and the resulting values are  $z_{\text{O}_1(\text{O}_2)} = 0.162$ ,  $z_{\text{O}_3} = 0.50$ , and  $z_{\text{Sr}_1(\text{Sr}_2)} = 0.353$ . The latter two values are in almost perfect agreement with experimental data,<sup>11</sup> only  $z_{\text{O}_1}$  is slightly smaller in our calculation. Very similar values are obtained already at the non-magnetic LDA level.

The density of states (DOS) of the G-type structure calculated within DFT+U (Fig. 2) shows that the Tc  $t_{2g}$  band is close to full polarization, with almost no occupied  $t_{2g}$  states in the minority channel. As the  $t_{2g}$  states extend also to the oxygen orbitals where the contribution to the spin density in the antiferromagnetic configuration cancel, the moment relevant to neutron measurements can be expected to be smaller. One may try to estimate this moment by looking at the spin polarization within MT spheres, which gives  $1.82 \mu_B$ . As the compound is quite itinerant, some of the spin density extends outside of the MT sphere and this value has to be considered as the lower bound on the magnetic moment.

One may also see that DFT+U gives insulating behavior for  $\text{Sr}_2\text{TcO}_4$ , with the gap of about  $1.4 \text{ eV}$ .

## B. DMFT results

For the relaxed structure of  $\text{Sr}_2\text{TcO}_4$  we performed DFT+DMFT calculations. In a paramagnetic state we find that the metal-to-insulator transition happens close to  $U = 2.3 \text{ eV}$ ,  $J = 0.3 \text{ eV}$ , with these parameters corresponding already to an insulating solution, while  $\text{SrTcO}_3$  is for the same parameters a paramagnetic metal. The difference between the two materials is due to a

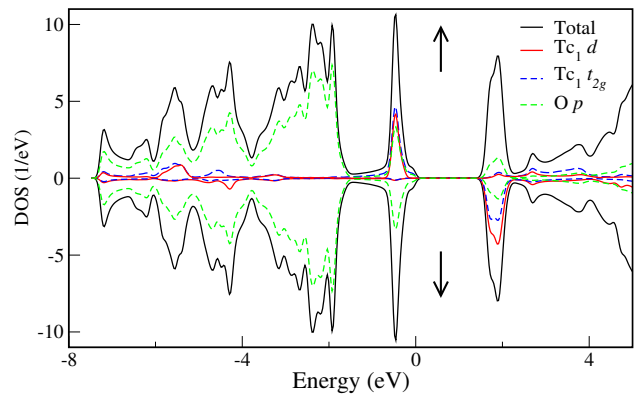


Figure 2. Total and partial Tc<sub>1</sub>  $d$ ,  $t_{2g}$  and O  $p$  DOS for the G-type AFM structure obtained by the GGA+U method for the theoretical equilibrium lattice structure.

smaller bandwidth of the quasi-two-dimensional compound  $\text{Sr}_2\text{TcO}_4$ .

On Fig. 3 we plot the orbitally projected DOS for  $\text{Sr}_2\text{TcO}_4$  as calculated within DFT+DMFT using Maximum Entropy for analytical continuation.<sup>44</sup> One can observe that especially for the  $xy$  orbital, the gap is very small, demonstrating that for the selected parameters, the compound is very close to the insulator-to-metal transition. On Fig. 3 (a), besides the paramagnetic DMFT DOS additionally the orbitally projected LDA DOS in the paramagnetic state are plotted. These show that bands spanned by the  $xz, yz$  orbitals are narrower, which explains the occurrence of a broader gap in the  $xz, yz$  DMFT DOS.

In passing we note that stronger correlations in  $xz, yz$  orbitals is opposite to what one finds in isostructural  $4d^4$  compound  $\text{Sr}_2\text{RuO}_4$ , where the strongest mass renormalization has been found in the  $xy$  orbital, due to proximity to the van-Hove singularity.<sup>45</sup>  $\text{Sr}_2\text{TcO}_4$ , being half-filled, is dominated by the proximity to the Mott transition, and the van-Hove singularity is further from the Fermi level, which both contribute to the fact that standard argument which associates the more narrow band with stronger correlations applies.

The fact that the compound is close to the metal-to-insulator transition in the paramagnetic state points to strong tendencies, as was discussed for  $\text{SrTcO}_3$ .<sup>5</sup> Actually, if in DMFT one allows for the magnetic ordering one gets a very similar behavior as in the case of  $\text{SrTcO}_3$  and similar DMFT ordering temperature about  $2000 \text{ K}$ . On Fig. 3(b) we plot the spin and orbitally resolved DMFT DOS calculated well in the antiferromagnetic state at  $T = 290 \text{ K}$ . Comparing to panel (a), one can notice that a bigger gap is opened by the onset of magnetic order. The size of the gap is comparable to the one found DFT+U (Fig. 2). Conversely, in pure local spin density approximation (LSDA) the gap in the antiferromagnetic state is very small and only about  $0.05 \text{ eV}$ .

The large ordering temperatures found in DMFT calculations should be taken as pointing to strong magnetic

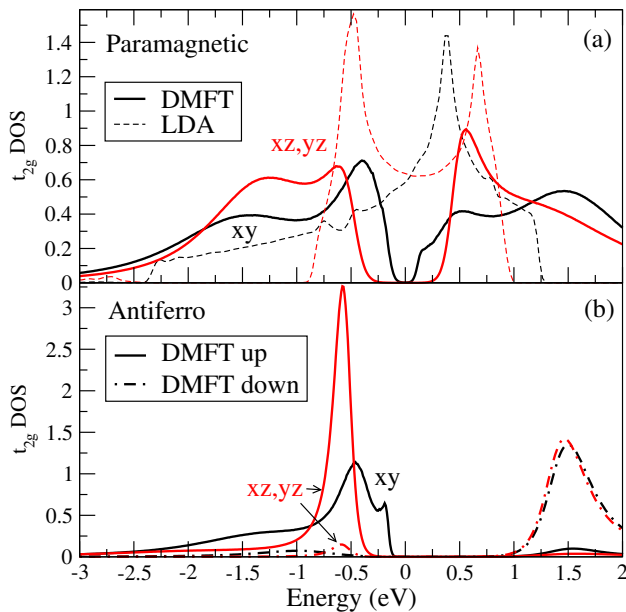


Figure 3. Orbitaly resolved DOS for  $t_{2g}$ -states in  $\text{Sr}_2\text{TcO}_4$  calculated from LDA+DMFT at temperature  $T = 290$  K, and from LDA. (a) Paramagnetic calculation. (b) Antiferromagnetic calculation.

correlations but cannot be trusted quantitatively. Furthermore, in quasi-2D these fluctuations become more important than in 3D, hence even relative comparison to the values found in  $\text{SrTcO}_3$  is meaningless.

One can, however, assume that the ordering takes place and calculate from DMFT the value of the ordered magnetic moment at low temperatures. Employing the same scheme as for  $\text{SrTcO}_3$ ,<sup>5</sup> i.e., calculating the moment in the set of localized d-p Wannier functions, results in a moment of  $2.1 \mu_B$ . Again, this is significantly smaller than the saturation value of  $3 \mu_B$ . The reason is partly due to covalence and partly due to charge fluctuations, which both arise from strong hybridization of Tc d with oxygen p states.

To investigate the ordering temperature itself one needs to employ other approaches that are more suitable for quasi-2D systems. We discuss this next.

### C. Exchange interactions and results of Monte Carlo simulations

In order to obtain theoretical exchange interactions we have employed two approaches: First, the one described in Sec. II C, and second, we also extracted nearest-neighbor  $J_{\text{DFT+U}}$  from the difference of GGA+U total energies between ferromagnetic and AFM structures (we chose AFM cubic and tetragonal structures with all nearest-neighbor transition metal sites having opposite spin directions).

In Table I we list our calculated and known experimental values of the spin exchange interactions, which

Table I. Calculated exchange interactions compared to the experimental values from the literature.

compound	$J$ [meV]	$J'$ [meV]	$J_{\text{DFT+U}}$ [meV]	$J_{\text{exp}}$ [meV]
$\text{KNiF}_3$	-12.7	-0.13	-7.7	-8 <sup>46</sup>
$\text{K}_2\text{NiF}_4$	-13.5	-0.13	-8.4	-8.6 <sup>46</sup>
$\text{Rb}_2\text{MnF}_4$	-	-	-1.1	-0.65 <sup>46</sup>
$\text{SrMnO}_3$	-8.1	-0.76	-9.1	-4.14 <sup>48</sup>
$\text{Sr}_2\text{MnO}_4$	-10.27	-0.83	-12.4	-6.89 <sup>48</sup>
$\text{SrTcO}_3$	-28.2	-0.9	-32.8	-
$\text{Sr}_2\text{TcO}_4$	-35.6	-0.9	-45.1	-

were obtained from neutron and Raman scattering experiments as described in Refs. 46 and 47. To our knowledge, only the exchange interactions for the first nearest neighbors have been measured experimentally in the compounds under consideration, except for  $\text{K}_2\text{NiF}_4$ , where the exchange coupling for the next-nearest neighbors is  $J'_{\text{exp}} = 0.5$  meV. One may notice that  $\text{Sr}_2\text{TcO}_4$  has exceptionally strong exchange couplings in comparison with other layered perovskites.

Comparing the theoretical values to the measured ones, one notices that the two approaches behave differently. DFT+U works well for the localized compounds; for the strongly localized Ni fluorides the calculated exchange interactions are in close agreement to experiment. The DFT+U estimates become progressively worse when the localization becomes weaker and the Mott insulator-to-metal transition is approached.

The DFT+HubI approach, on the other hand, gives values that are approximately 50% larger than the experimental values irrespectively of the vicinity of the Mott transition point.<sup>49</sup> For “ionic” Ni fluorides, less localized Mn perovskites, and most itinerant  $\text{SrTcO}_3$  one observes similar relative overestimate. As our aim is to predict the transition temperature and furthermore for the compound that is close to the Mott transition, we employed the DFT+HubI values for  $J$  Monte Carlo calculations described in the following.

The critical temperatures computed within the classical Monte Carlo approach for the set of cubic and layered perovskites are reported in Table II. In the first four columns we present results of numerical simulations and in the last column we list the known experimental values of critical temperatures. In the first column we list calculated critical temperatures (denoted by  $T_0$ ) for experimentally determined exchange interactions and mapping  $\alpha_1 = S(S+1)$ . In our evaluation of the critical temperature for experimental interactions, we calculated  $J'$  (when it was not available from experiment) by multiplying  $J_{\text{exp}}$  with the ratio  $J'/J$  of theoretical values. For layered perovskites, we added the long-range dipolar interaction as described in Sec. (II E). Results in columns  $T_0, T_{\text{exp}}$  are in very good agreement, which supports the choice of  $\alpha_1$  in the quantum to classical mapping.

In columns  $T^{(\alpha_1)}, T^{(\alpha_2)}, T^{(\alpha_3)}$  we present critical temperatures for theoretical values of exchange interactions

Table II. In column  $T_0$  we list calculated critical temperatures for experimental values of exchange interactions  $J$ .  $T^{(\alpha_1)}$ ,  $T^{(\alpha_2)}$ ,  $T^{(\alpha_3)}$  are critical temperatures for theoretically calculated exchange interactions  $J$ , and  $T_{\text{exp}}$  are experimentally measured critical temperatures.

compound	$T_0$ [K]	$T^{(\alpha_1)}$ [K]	$T^{(\alpha_2)}$ [K]	$T^{(\alpha_3)}$ [K]	$T_{\text{exp}}$ [K]
KNiF <sub>3</sub>	259	410	307	205	253 <sup>17</sup>
K <sub>2</sub> NiF <sub>4</sub>	105	166	124	83	97.1 <sup>50</sup>
Rb <sub>2</sub> MnF <sub>4</sub>	39.8	-	-	-	38.5 <sup>18</sup>
SrMnO <sub>3</sub>	259	370	296	222	260 <sup>51</sup>
Sr <sub>2</sub> MnO <sub>4</sub>	162	212	170	127	170 <sup>48</sup>
SrTcO <sub>3</sub>	-	1610	1286	965	1023 <sup>1</sup>
Sr <sub>2</sub> TcO <sub>4</sub>	-	720	630	430	-

and mappings  $\alpha_1 = S(S+1)$ ,  $\alpha_2 = S(S+1/2)$ ,  $\alpha_3 = S^2$ , respectively.

From Table II it is obvious that the calculations of the exchange interactions are not precise enough to allow for direct prediction of the transition temperature. However, the deviations are systematic and therefore we can estimate from joint theoretical and experimental data the transition temperature of Sr<sub>2</sub>TcO<sub>4</sub>. We extrapolate from the comparison between the theory and experiment on similar compounds (that furthermore all have  $S = 3/2$ ), in order that systematic error (the “correct” choice of  $\alpha$ ) drops out. It is convenient to introduce the notation

$$T_x(a; b) = T^{(\alpha)}(a) \frac{T_{\text{exp}}(b)}{T^{(\alpha)}(b)} \quad (5)$$

that describes the predicted temperature  $T_x$  for compound  $a$  corrected by the ratio of experimental and theoretical values evaluated on a compound  $b$ . Using that notation, one has  $T_x(\text{Sr}_2\text{TcO}_4; \text{SrTcO}_3) = 456$  K and  $T_x(\text{Sr}_2\text{TcO}_4; \text{Sr}_2\text{MnO}_4) = 576$  K. Averaging those two results gives 500 K with 50 K errorbar. Using other entries of Table II for the reference compound  $b$  does not change the result significantly. We also note that for all the investigated compounds, the measured transition temperatures  $T_{\text{exp}}$  are between  $T^{(\alpha_2)}$  and  $T^{(\alpha_3)}$ , therefore these two latter values can be used as the (somewhat rougher) upper and lower limit for the predicted transition temperature within our approach, too.

#### IV. DISCUSSION

Another reason for the magnetic ordering in the layered perovskites of the K<sub>2</sub>NiF<sub>4</sub> type is the single-ion anisotropy<sup>17,50</sup> that originates in the combination of spin-orbit interactions and the tetragonal crystal field. Whereas spin-orbit interaction is sizable in 4d oxides its effects are expected to be less important here because in the present case of half-filled  $t_{2g}$  orbitals the total orbital momentum vanishes. Nevertheless, we calculated the ordering temperature also in the presence of additional single-ion magnetic anisotropy and found that its

effects are not important (a 100% increase of anisotropy above the value that is already effectively present due to the dipole-dipole interactions causes only 3% increase of the critical temperature).

We investigated the effects of the direct next-nearest layer coupling, too. Within our approach we estimate that this coupling is very small, i.e.  $\approx 0.01$  meV. Including this interaction increases the transition temperature by about 50 K, from which follows our final prediction 550 K with 50 K errorbar.

Finally, the orthorhombic distortion (that has not been reported experimentally so far, and hence we did not include it), might lead also to significant reduction of the frustration of the magnetic couplings between the layers. This effect would make the magnetic transition more of the La<sub>2</sub>CuO<sub>4</sub> kind,<sup>52</sup> and would increase the transition temperature further. Our DFT+U simulations, Sec. III A, predict that sizable orthorhombic distortions do not occur. If such distortions were realized in the real structure nevertheless, then our results should be taken as an estimate of the lower bound of the transition temperature.

#### V. CONCLUSIONS

In summary, using a newly developed combination of theoretical methods that we tested on a set of cubic and layered perovskites, we investigated properties of the single-layer technetium perovskite Sr<sub>2</sub>TcO<sub>4</sub>. The calculated in-plane exchange interactions are large, which establishes Sr<sub>2</sub>TcO<sub>4</sub> as a strong 2D magnet. We predict the long range AFM order to occur (despite the complete frustration of the inter-plane exchange) due to the effective spin anisotropy that originates in the dipole-dipole interactions. We estimate the ordering temperature to be in the 500-600 K range.

We note that it would be interesting to dope this compound. Namely, Sr<sub>2</sub>TcO<sub>4</sub> is according to our predictions a strong antiferromagnet, but the magnetic order must disappear upon doping with electrons, as Sr<sub>2</sub>RuO<sub>4</sub> is known to be a (low-spin) paramagnet that becomes an unconventional superconductor below 1.5 K. Similar would happen on doping with holes, as SrMoO<sub>3</sub> is paramagnetic, too. In cuprates, strong magnetic interactions in a doped compound in which magnetic order disappears lead to an unusual electronic state and high-temperature superconductivity.<sup>53</sup> From iron-based superconductors, we learned that the high-temperature superconductivity is possible also in a multi-orbital context.<sup>54</sup> In doped Tc compounds similar, or other interesting discoveries may be ahead. In this respect, not only investigations on layered Tc compounds<sup>11</sup> but also the attempts of material synthesis of half-filled  $t_{2g}$  shell perovskites<sup>55,56</sup> are extremely interesting.

## ACKNOWLEDGMENTS

We warmly thank Antoine Georges for stimulating and helpful discussions. L.P. acknowledges computational resources provided by the Swedish National Infrastructure for Computing (SNIC) at National Supercomputer Centre (NSC) and PDC Centre for High Performance Computing (PDC-HPC). M.A. is supported by the Austrian Science Fund FWF, projects F04103 and Y746. J.M and A.H. acknowledge support of Slovenian research agency under program P1-0044.

### Appendix A: Calculation of magnetic interactions within DFT+DMFT

In the case of  $\text{Tc}^{4+}$  and other transition-metal ions with a ground-state (GS) multiplet well separated from excited states, the Hubbard-I atomic Green's function (GF) at low temperature has a particularly simple form  $G_{\text{at}}(i\omega_n) = \sum_{\Gamma} G_{\Gamma}(i\omega_n)w_{\Gamma}$ . The matrix elements  $G_{\Gamma}^{\sigma,mm'}$  of the contribution due to the state  $\Gamma$  of the GS multiplet are given (in the imaginary time domain) by  $-\langle \Gamma | T [c_{\sigma m}(\tau)c_{\sigma m'}^{\dagger}(0)] | \Gamma \rangle$ , where  $c_{\sigma m}^{(\dagger)}$  are annihilation (creation) operators for the spin  $\sigma$  and magnetic quantum number  $m$ ,  $T$  is the time-ordering operator.  $w_{\Gamma}$  are the weights of states within the GS multiplet, their ‘‘atomic’’

values at low temperature (and in absence of crystal-field splitting) are simply given by  $1/N$ , where  $N$  is the GS multiplicity.

However, one may consider  $G_{\text{at}}$  (and the corresponding self-energy  $\Sigma_{\text{at}}$  related to  $G_{\text{at}}$  by the Dyson equation) as a function of  $w_{\Gamma}$ . By writing the DFT+DMFT free energy in the standard form<sup>57</sup> as a functional of the local self-energy and GF, introducing small fluctuations of  $w_{\Gamma}^{i(j)}$  with respect to their ‘‘atomic’’ value on two neighboring sites  $i(j)$  and then computing the linear response of the free energy due to the fluctuation  $\delta w_{\Gamma}^i \delta w_{\Gamma}^j$ , one obtains the corresponding matrix element of  $\langle \Gamma_i \Gamma_j' | \mathcal{H}_{le} | \Gamma_i \Gamma_j' \rangle$  of a low-energy spin-orbital Hamiltonian  $\mathcal{H}_{le}$ . In the present case of half-filled TM ions (e.g.  $\text{Tc}^{4+}$ ) the atomic states  $\{\Gamma\}$  are in fact just different eigenstates of the  $S_z$  operator, and the resulting matrix elements are those of the quantum Heisenberg Hamiltonian Eq. (1), from which  $J_{ij}$  are easily obtained. Detailed description of the method will be given in a separate publication.<sup>58</sup>

In DFT+HubI calculations of Tc perovskites within Hubbard-I we employed the values of orbital on-site  $U = 2.3\text{eV}$  and  $J_H = 0.3\text{eV}$ , as described in the text. For other compounds considered we have selected the values (in eV) of  $U$ ,  $J_H$  consistent with available literature data: 3.5,0.6 for  $\text{SrMnO}_3$  and  $\text{Sr}_2\text{MnO}_4$ ; 9.1,0.7 for  $\text{KNiF}_3$  and  $\text{K}_2\text{NiF}_4$ ; 5.1,0.7 for  $\text{Rb}_2\text{MnF}_4$ .

- 
- <sup>1</sup> E. E. Rodriguez, F. Poineau, A. Llobet, B. J. Kennedy, M. Avdeev, G. J. Thorogood, M. L. Carter, R. Seshadri, D. J. Singh, and A. K. Cheetham, *Phys. Rev. Lett.* **106**, 067201 (2011).
  - <sup>2</sup> M. Avdeev, G. J. Thorogood, M. L. Carter, B. J. Kennedy, J. Ting, D. J. Singh, and K. S. Wallwork, *J. Am. Chem. Soc.* **133**, 1654 (2011).
  - <sup>3</sup> L. de' Medici, J. Mravlje, and A. Georges, *Phys. Rev. Lett.* **107**, 256401 (2011).
  - <sup>4</sup> C. Franchini, T. Archer, J. He, X.-Q. Chen, A. Filippetti, and S. Sanvito, *Phys. Rev. B* **83**, 220402 (2011).
  - <sup>5</sup> J. Mravlje, M. Aichhorn, and A. Georges, *Phys. Rev. Lett.* **108**, 197202 (2012).
  - <sup>6</sup> S. Middey, A. K. Nandy, S. K. Pandey, P. Mahadevan, and D. D. Sarma, *Phys. Rev. B* **86**, 104406 (2012).
  - <sup>7</sup> G. Wang, L. Li, C. Liu, M. Zhang, and Z. Yang, *Phys. Lett. A* **376**, 3313 (2012).
  - <sup>8</sup> C.-M. Dai and C.-L. Ma, *Mod. Phys. Lett.* **28**, 1450049 (2014).
  - <sup>9</sup> A. Georges, L. de' Medici, and J. Mravlje, *Annu. Rev. Condens. Matter Phys.* **4**, 137 (2013) **4**, 137 (2013).
  - <sup>10</sup> W. Pies and A. Weiss, ‘‘Landolt-bornstein - group iii condensed matter,’’ Chap. f2694, XX.2.1 Simple oxo-compounds of technetium (oxotechnetates).
  - <sup>11</sup> T. Hartmann, A. J. Alaniz, and D. J. Antonio, *Proc. Chem.* **7**, 622 (2012).
  - <sup>12</sup> N. D. Mermin and H. Wagner, *Phys. Rev. Lett.* **17**, 1133 (1966).
  - <sup>13</sup> S. Chakravarty, B. I. Halperin, and D. R. Nelson, *Phys. Rev. B* **39**, 2344 (1989).
  - <sup>14</sup> D. J. Scalapino, Y. Imry, and P. Pincus, *Phys. Rev. B* **11**, 2042 (1975).
  - <sup>15</sup> H. J. Schulz, *Phys. Rev. Lett.* **77**, 2790 (1996).
  - <sup>16</sup> C. Yasuda, S. Todo, K. Hukushima, F. Alet, M. Keller, M. Troyer, and H. Takayama, *Phys. Rev. Lett.* **94**, 217201 (2005).
  - <sup>17</sup> M. Lines, *Phys. Rev.* **164**, 736 (1967).
  - <sup>18</sup> C. Zhou, D. Landau, and T. Schulthess, *Phys. Rev. B* **76**, 024433 (2007).
  - <sup>19</sup> R. A. Cowley, G. Shirane, R. J. Birgeneau, and H. J. Guggenheim, *Phys. Rev. B* **15**, 4292 (1977).
  - <sup>20</sup> R. J. Christianson, R. L. Leheny, R. J. Birgeneau, and R. W. Erwin, *Phys. Rev. B* **63**, 140401 (2001).
  - <sup>21</sup> D. P. Landau and K. Binder, *A guide to Monte Carlo simulations in statistical physics* (Cambridge university press, 2009).
  - <sup>22</sup> U. Rößler, *Phys. Rev. B* **59**, 13577 (1999).
  - <sup>23</sup> P. Blaha, K. Schwarz, G. Madsen, D. Kvasnicka, and J. Luitz, *WIEN2k, An augmented Plane Wave + Local Orbitals Program for Calculating Crystal Properties* (Techn. Universität Wien, Austria, ISBN 3-9501031-1-2., 2001).
  - <sup>24</sup> DFT+U calculations were carried out using the implementation of the Wien2k package within GGA approximation. The correlated orbitals used in this implementation are different from those employed in the TRIQS package, hence, we employed slightly different values of  $U$  in our DFT+DMFT and DFT+U calculations of  $\text{Sr}_2\text{TcO}_4$ .
  - <sup>25</sup> V. I. Anisimov, I. V. Solov'yev, M. A. Korotin, M. T.

- Czyżyk, and G. A. Sawatzky, *Phys. Rev. B* **48**, 16929 (1993).
- <sup>26</sup> J. P. Perdew, K. Burke, and M. Ernzerhof, *Phys. Rev. Lett.* **77**, 3865 (1996).
- <sup>27</sup> M. Ferrero and O. Parcollet, “Triqs: a toolkit for research in interacting quantum systems,” [Http://ipht.cea.fr/triqs](http://ipht.cea.fr/triqs).
- <sup>28</sup> M. Aichhorn *et al.*, *Phys. Rev. B* **80**, 085101 (2009).
- <sup>29</sup> M. Aichhorn, L. Pourovskii, and A. Georges, *Phys. Rev. B* **84**, 054529 (2011).
- <sup>30</sup> E. Gull, A. J. Millis, A. I. Lichtenstein, A. N. Rubtsov, M. Troyer, and P. Werner, *Rev. Mod. Phys.* **83**, 349 (2011).
- <sup>31</sup> P. Werner and A. J. Millis, *Phys. Rev. B* **74**, 155107 (2006).
- <sup>32</sup> L. Boehnke, H. Hafermann, M. Ferrero, F. Lechermann, and O. Parcollet, *Phys. Rev. B* **84**, 075145 (2011).
- <sup>33</sup> N. Parragh, A. Toschi, K. Held, and G. Sangiovanni, *Phys. Rev. B* **86**, 155158 (2012).
- <sup>34</sup> J. Hubbard, *Proc. Roy. Soc. (London)* **A 276**, 238 (1963).
- <sup>35</sup> A. Liechtenstein, M. Katsnelson, V. Antropov, and V. Gubanov, *J. Magn. Magn. Mater.* **67**, 65 (1987).
- <sup>36</sup> P. Bruno, *Phys. Rev. Lett.* **90**, 087205 (2003).
- <sup>37</sup> A. V. Ruban, S. Shallcross, S. I. Simak, and H. L. Skriver, *Phys. Rev. B* **70**, 125115 (2004).
- <sup>38</sup> M. I. Katsnelson and A. I. Lichtenstein, *Phys. Rev. B* **61**, 8906 (2000).
- <sup>39</sup> X. Wan, Q. Yin, and S. Y. Savrasov, *Phys. Rev. Lett.* **97**, 266403 (2006).
- <sup>40</sup> G. Rushbrooke and P. Wood, *Mol. Phys.* **6**, 409421 (1963).
- <sup>41</sup> J. Oitmaa and W. Zheng, *J. Phys. Condens. Matter* **16**, 8653 (2004).
- <sup>42</sup> R. Martin and F. Illas, *Phys. Rev. Lett.* **79**, 1539 (1997).
- <sup>43</sup> T. Archer, C. D. Pemmaraju, S. Sanvito, C. Franchini, J. He, A. Filippetti, P. Delugas, D. Puggioni, V. Fiorentini, R. Tiwari, and P. Majumdar, *Phys. Rev. B* **84**, 115114 (2011).
- <sup>44</sup> K. S. D. Beach, “Identifying the maximum entropy method as a special limit of stochastic analytic continuation,” [Cond-mat/0403055](https://arxiv.org/abs/cond-mat/0403055).
- <sup>45</sup> J. Mravlje, M. Aichhorn, T. Miyake, K. Haule, G. Kotliar, and A. Georges, *Phys. Rev. Lett.* **106**, 096401 (2011).
- <sup>46</sup> L. de Jongh and A. Miedema, *Adv. Phys.* **23**, 1 (1974).
- <sup>47</sup> P. Fleury and R. Loudon, *Phys. Rev.* **166**, 514 (1968).
- <sup>48</sup> J.-C. Bouloux, J.-L. Soubeyroux, G. L. Flem, and P. Hängguller, *J. Solid State Chem.* **38**, 34 (1981).
- <sup>49</sup> A significant overestimation of the inter-site exchange within an approach based on Hubbard-I has been previously pointed out in Ref. 39. Apparently, neglecting hybridization effects in calculation of the impurity Green’s function is a rather crude approximation even for strongly-localized Mott insulators.
- <sup>50</sup> R. Birgeneau, H. Guggenheim, and G. Shirane, *Phys. Rev. B* **1**, 2211 (1970).
- <sup>51</sup> T. Takeda and S. Ōhara, *J. Phys. Soc. Jpn.* **37**, 275 (1974).
- <sup>52</sup> M. Kastner, R. Birgeneau, G. Shirane, and Y. Endoh, *Rev. Mod. Phys.* **70**, 897 (1998).
- <sup>53</sup> E. Dagotto, *Rev. Mod. Phys.* **66**, 763 (1994).
- <sup>54</sup> J. Paglione and R. L. Greene, *Nature Phys.* **6**, 645 (2010).
- <sup>55</sup> C. I. Hiley, M. R. Lees, J. M. Fisher, D. Thompsett, S. Agrestini, R. I. Smith, and R. I. Walton, *Angewandte Chemie* **126**, 4512 (2014).
- <sup>56</sup> H. Seki, R. Yamada, T. Saito, B. J. Kennedy, and Y. Shimakawa, *Inorg. Chem.* **53**, 4579 (2014).
- <sup>57</sup> S. Y. Savrasov and G. Kotliar, *Phys. Rev. B* **69**, 245101 (2004).
- <sup>58</sup> L. Pourovskii, In preparation.